

and growth of the metal nanoclusters preferentially occur. Consequently, the size of the resulting nanoparticles matches the dimension of the nanometer-sized cavities inside these swollen domains. The possibility of controlling the growth of the metal nanoclusters by changing the morphological features of the support represents a unique feature of resin supports, in which the metal nanoparticles are generated *inside* the swollen polymer network and not simply at its surface. It can be inferred that functional resins characterized by a narrower distribution of nanoporous domains will make it possible to control even more precisely the size and size distribution of the metal nanoclusters generated inside them, a task that we are going to turn to in the near future.

### Experimental

Solvents and chemicals were of reagent grade and were used as received. XRM analyses were obtained with a Cambridge Stereoscan 250 EDX PW 9800 apparatus. TEM micrographs were obtained using a Philips CM100 microscope. ISEC measurements were carried out using an established procedure and a standard chromatographic set-up described elsewhere [13,14]. The ESR spectra were recorded on an X-band JEOL JES-RE1X apparatus at 9.2 GHz (modulation 100 kHz). Details of sample preparation and measurement have been reported elsewhere [18].

**Resin Preparation:** Monomers were mixed in the desired ratios and the resulting mixtures (10 g) were diluted with 5–10 % w/w dimethylformamide in order to ensure complete miscibility. They were exposed to the  $\gamma$ -rays from a  $^{60}\text{Co}$  source at  $0.5 \text{ Gys}^{-1}$  at room temperature and at a distance of 21 cm for 72 h. The resulting clear transparent rods were crushed, extensively washed with methanol, acetone, and diethylether, vacuum dried, and sieved to a particle size  $<0.18 \text{ mm}$ .

**Impregnation with Pd:** Resin (2 g) was added to a solution of 44 mg  $\text{Pd}(\text{OAc})_2$  (1 % by weight of Pd with respect to the polymer) in 50 mL tetrahydrofuran (THF)/water 4/1. The suspension was stirred overnight, then the resin was filtered off, washed thoroughly with THF and diethylether and allowed to dry in air.

**Pd Reduction:** Exchanged resin (1 g) was swollen in ethanol (20 mL) for 1 h. A solution of  $\text{NaBH}_4$  (0.14 g) in ethanol (40 mL) was added and the resulting suspension stirred overnight. The resin was filtered off, washed with ethanol and THF, and dried under vacuum at room temperature to constant weight.

Received: May 29, 2000

- [1] *Clusters and Colloids* (Ed: G. Schmid), VCH, Weinheim **1994**.  
 [2] C. N. R. Rao, G. U. Kulkarni, P. J. Thomas, P. P. Edwards, *Chem. Soc. Rev.* **2000**, 29, 27.  
 [3] J. D. Aiken III, R. G. Finke, *J. Mol. Catal. A: Chem.* **1999**, 145, 1.  
 [4] G. Schmid, L. F. Chi, *Adv. Mater.* **1998**, 10, 515.  
 [5] A. Henglein, *Chem. Rev.* **1989**, 89, 1861.  
 [6] G. Schmid, *Chem. Rev.* **1992**, 92, 1709.  
 [7] L. N. Lewis, *Chem. Rev.* **1993**, 93, 2693.  
 [8] a) M. Králik, M. Hronec, S. Lora, G. Palma, M. Zecca, A. Biffis, B. Corain, *J. Mol. Catal. A: Chem.* **1995**, 97, 145. b) M. Králik, M. Hronec, V. Jorik, S. Lora, G. Palma, M. Zecca, A. Biffis, B. Corain, *J. Mol. Catal. A: Chem.* **1995**, 101, 143. c) A. Biffis, B. Corain, Z. Cvengrosová, M. Hronec, K. Jerábek, M. Králik, *Appl. Catal. A: Chem.* **1995**, 124, 355. d) A. Biffis, H. Landes, K. Jerábek, B. Corain, *J. Mol. Catal. A: Chem.* **2000**, 151, 283.  
 [9] a) N. H. Li, J. M. J. Frechet, *React. Polym.* **1987**, 6, 311. b) K. Jerábek *J. Mol. Catal.* **1989**, 55, 247. c) T. Teranishi, N. Toshima, *J. Chem. Soc., Dalton Trans.* **1994**, 2967. d) A. L. Rusanov, M. E. Vol'pin, A. A. Belyi, L. G. Chigladze, *Macromol. Symp.* **1994**, 80, 215. e) R. Fisera, M. Králik, J. Annus, V. Kratky, M. Zecca, M. Hronec, *Collect. Czech. Chem. Commun.* **1997**, 62, 1763. f) Z. M. Michalska, B. Ostaszewski, J. Zientarska, J. W. Sobczak, *J. Mol. Catal. A: Chem.* **1998**, 129, 207. g) D. Gasparovicova, M. Králik, M. Hronec, *Collect. Czech. Chem. Commun.* **1999**, 64, 502. h) A. Drelinkiewicz, M. Hasik, M. Kloc, *J. Catal.* **1999**, 186, 123. i) M. Zecca, R. Fisera, G. Palma, S. Lora, M. Hronec, M. Králik, *Chem. Eur. J.* **2000**, 6, 1980.  
 [10] J. Wöllner, W. Neier, *German Patent 1 260 454*, **1969**.  
 [11] *Bayer Polymer-Based Catalysts. Properties and Applications*, Bayer AG **1989**.

- [12] R. Arshady, *Adv. Mater.* **1991**, 3, 182.  
 [13] K. Jerábek, in *Cross Evaluation of Strategies in Size-Exclusion Chromatography*, ACS Symposium Series 635, American Chemical Society, Washington, DC **1996**, p. 211.  
 [14] K. Jerábek, *Anal. Chem.* **1985**, 57, 1598.  
 [15] G. Ogston, *Trans. Faraday Soc.* **1958**, 54, 1754.  
 [16] a) A. Biffis, B. Corain, M. Zecca, C. Corvaja, K. Jerábek, *J. Am. Chem. Soc.* **1995**, 117, 1603. b) M. Zecca, A. Biffis, G. Palma, C. Corvaja, S. Lora, K. Jerábek, B. Corain, *Macromolecules* **1996**, 29, 4655. c) A. A. D'Archivio, L. Galantini, A. Panatta, E. Tettamanti, B. Corain *J. Phys. Chem. B* **1998**, 102, 6779.  
 [17] A. Guyot, in *Synthesis and Separations Using Functional Polymers* (Eds: D. C. Sherrington, P. Hodge), Wiley, New York **1988**, p. 1.  
 [18] A. A. D'Archivio, L. Galantini, A. Biffis, K. Jerábek, B. Corain, *Chem. Eur. J.* **2000**, 6, 794.

### Do Zeolites Have Negative Poisson's Ratios?\*

By Joseph N. Grima, Rosie Jackson, Andrew Alderson, and Kenneth E. Evans\*

Materials with a negative Poisson's ratio ( $\nu$ ), so-called auxetic materials, exhibit the unusual property of becoming wider when stretched and narrower when compressed.<sup>[1,2]</sup> A range of auxetic materials and structures have been discovered, fabricated or synthesized within the last decade.<sup>[1–10]</sup> Auxetic materials can possess enhancements in many materials properties<sup>[1,2,11]</sup> and consequently they have potential in many practical applications.<sup>[12,13]</sup> One area attracting increasing interest is the development of molecular auxetics.<sup>[4–7]</sup> These are expected to lead to high modulus auxetic materials as well as having potential in sensor, molecular sieve, and separation technologies.<sup>[12,13]</sup> Naturally occurring molecular auxetics<sup>[8–10]</sup> include  $\alpha$ -cristobalite in which auxetic behavior is thought to be due to the cooperative rotation of the  $\text{SiO}_4$  molecular tetrahedra making up the framework structure.<sup>[9,10]</sup> Zeolites are another important class of polyhedral framework nanostructures and are commonly used as molecular sieves because of their availability and their well-defined molecular-sized cavities and pathways.<sup>[14,15]</sup> We report here predictions, from force-field-based molecular modeling calculations, that several idealized zeolitic cage structures possess negative Poisson's ratios. In most of these idealized molecular structures, the auxetic behavior can be explained through a combination of the framework geometry and simple deformation mechanisms acting within the framework.

[\*] Prof. K. E. Evans, J. N. Grima  
 Dept. of Engineering, University of Exeter  
 North Park Road, Exeter EX4 4QF (UK)  
 E-mail: k.e.evans@ex.ac.uk

R. Jackson  
 School of Computing and Mathematical Sciences  
 Liverpool John Moores University  
 James Parsons Building  
 Byrom Street, Liverpool L3 3AF (UK)  
 Dr. A. Alderson  
 Faculty of Technology, Bolton Institute  
 Deane Road, Bolton BL3 5AB (UK)

[\*\*] JNG thanks the CVCP for awarding him an ORS award. RJ acknowledges support in the form of a one year student placement with BNFL.

The Poisson's ratio ( $\nu_{yx}$ ) of a material is given by:

$$\nu_{yx} = -\left(\frac{\text{lateral strain}}{\text{tensile strain}}\right) = -\frac{\varepsilon_x}{\varepsilon_y} \quad (1)$$

where  $\varepsilon_y$  is the strain in the direction of a uniaxially applied load (in the  $y$ -direction) and  $\varepsilon_x$  is the resulting strain in a transverse direction (the  $x$ -direction). In conventional materials  $\varepsilon_x$  is negative (contracts) when  $\varepsilon_y$  is positive (extended) and hence  $\nu_{yx}$  is generally positive. However, negative Poisson's ratios, in which  $\varepsilon_x$  and  $\varepsilon_y$  have the same sign, are allowed within classical elasticity theory.<sup>[16]</sup> In recent years several auxetics have been fabricated by modifying the microstructure of existing materials, e.g., foams<sup>[1]</sup> and microporous polymers,<sup>[3]</sup> whilst some examples of molecular auxetics have been proposed<sup>[4–7]</sup> and discovered.<sup>[8–10]</sup>  $\alpha$ -Cristobalite is an example, at the molecular level, of how negative on-axis Poisson's ratios can be achieved by geometrical re-arrangement of the structural sub-units ( $\text{SiO}_4$  tetrahedra) known to give positive on-axis Poisson's ratios in an alternative geometry (e.g.,  $\alpha$ -quartz<sup>[17]</sup>).

Materials property enhancements as a consequence of a negative Poisson's ratio include, for example, increased indentation resistance<sup>[11]</sup> and a natural ability to form synclastic (i.e., dome-shaped) surfaces.<sup>[1]</sup> A host of potential applications have been identified such as smart rivets having an increased grip upon loading, doubly curved aircraft nose cones,<sup>[2]</sup> and as components in enhanced-sensitivity piezoelectric devices for use in medical ultrasonic imagers and hydrophones for naval sonar.<sup>[8,18]</sup> Most recently, their application as tunable filters and sieves has been considered.<sup>[12,19]</sup> Auxetic sieves have the advantage of allowing control of the pore size, since the pore size in auxetic materials increases on application of a tensile load, leading to particulate size selectivity and de-fouling possibilities not amenable to the non-auxetic counterparts.

At the molecular level we expect zeolites to be a candidate class of materials for auxetic behavior in view of their open framework structures. Zeolites are aluminosilicate framework structures containing molecular-sized cages and channels formed from an array of corner-sharing  $\text{SiO}_4^{4-}$  and  $\text{AlO}_4^{5-}$  tetrahedra. In order to counteract the charge imbalance due to the extra negative charge on the  $\text{AlO}_4$  tetrahedra, an equivalent amount of cations are located within the cavities of the framework structures. The presence of cations and the molecular-sized pores in the structure lead to the use of zeolites in, for example, molecular sieve and ion exchange applications, providing added technological impetus to study their potential as molecular auxetics.

Although many zeolite properties have been thoroughly investigated, very little research has been performed on their single-crystal mechanical properties, primarily because of the problem of obtaining crystals more than a few micrometers in size.<sup>[20]</sup> It is well known that in order to reproduce the subtleties of the structure of zeolites it is necessary to include a description of polarization. It has been shown that ionic models derived for silica can be applied to a wide variety of zeolites

when the models are combined with polarizable ions.<sup>[21–23]</sup> However, whilst an ionic model employing formal charges on all ions with polarization effects accounted for has been found to be superior to partial-charge ionic models in reproducing the crystal structure of berlinite (an aluminophosphate), no appreciable improvements in the predicted elastic, dielectric, piezoelectric, and phonon properties were observed.<sup>[24]</sup> Hence, whilst accounting for polarization effects appears to be important in accurately predicting the structure of zeolites, it does not appear to be as important in predicting zeolite properties. We, therefore, expect Poisson's ratios and other elastic constants of zeolites to be reasonably well predicted by force fields that are appropriate for modeling the elastic constants of silica.

We have used the Cerius<sup>2</sup> molecular modeling software<sup>[25]</sup> to perform force-field-based simulations on a large number of idealized zeolite frameworks. Due to the absence of a significant body of experimental data with which to validate force fields for the prediction of the mechanical properties of single-crystal zeolite structures, a variety of force fields specifically parameterized to model other zeolite properties were employed to calculate the stiffness matrix  $\mathbf{C}$ . The on-axis Poisson's ratios and other elastic constants may be obtained directly from the compliance matrix,  $\mathbf{S} = \mathbf{C}^{-1}$ , since for example  $\nu_{ij} = -s_{ij}/s_{ii}$ . The off-axis Poisson's ratios may be similarly derived from the transformed stiffness matrix  $\mathbf{C}$  derived through using standard transformation relationships.<sup>[26]</sup>

In the simulations, the Burchart,<sup>[27]</sup> BKS,<sup>[28]</sup> Universal,<sup>[29,30]</sup> and CVFF (a proprietary force field)<sup>[31]</sup> (CVFF = consistent valence force field) force fields were used. The Burchart force field assumes the frameworks are largely covalent and was developed specifically to model the properties of silicas and aluminophosphates. Interactions were parameterized using experimental data. The BKS force field was also developed specifically for silicas and aluminophosphates, with parameterization based on both experimental and ab initio data. The BKS force field treats interatomic interactions as ionic rather than covalent. The Universal force field is a purely diagonal, harmonic force field developed to cover the whole of the periodic table. Parameterization is based on prescribed equations to combine atomic parameters so that any combination of atom types can be considered.<sup>[29]</sup> The CVFF is a generalized valence force field that includes non-bond parameters for use in simulations of silicates, aluminosilicates, clays, and aluminophosphates.

Frameworks were modeled in the absence of cations within the framework structures. Hence it was necessary to perform charge neutralization procedures for non-purely siliceous structures. In an alternative approach analogous all-silica zeolite structures were considered where, for example, Al atoms were replaced by Si atoms to ensure charge neutrality for the framework.

In order to validate the accuracy of the force fields and methods employed the elastic constants for the auxetic  $\alpha$ -cristobalite polymorph of crystalline silica were modeled and

compared with experimental values.<sup>[9]</sup> The elastic constants for zeolite SOD (sodalite—Al<sub>6</sub>Si<sub>6</sub>O<sub>24</sub>), for which there are experimental data,<sup>[32]</sup> were also calculated.

Table 1 compares the experimental Poisson's ratios and Young's moduli for single-crystal  $\alpha$ -cristobalite and SOD with those calculated using the four force fields referred to above.

Table 1. Comparison of experimental and calculated elastic constants for  $\alpha$ -cristobalite and SOD (sodalite—Al<sub>6</sub>Si<sub>6</sub>O<sub>24</sub>). Also shown are the polycrystalline isotropic aggregate values of Poisson's ratio ( $\nu_{\text{Voigt}}$ ), averaged using the Voigt method [33]. Calculated errors are  $\pm 5\%$ .

	$\nu_{xy}$	$\nu_{xz}$	$\nu_{zx}$	$\nu_{\text{Voigt}}$	$E_x$ [GPa]	$E_z$ [GPa]
<b><math>\alpha</math>-Cristobalite</b>						
Experiment	+0.06 ( $\pm 0.01$ )	-0.10 ( $\pm 0.02$ )	-0.07 ( $\pm 0.01$ )	-0.19 ( $\pm 0.01$ )	58.8 ( $\pm 0.5$ )	41.8 ( $\pm 0.7$ )
Burchart	+0.20	+0.02	+0.009	+0.03	100.0	45.7
BKS	+0.16	+0.07	+0.05	-0.06	68.0	46.7
Universal	+0.11	+0.14	+0.08	+0.11	285.7	166.7
CVFF	+0.09	-0.16	-0.07	-0.05	142.9	66.20
<b>SOD</b>						
Experiment	+0.304 ( $\pm 0.003$ )	+0.304 ( $\pm 0.003$ )	+0.304 ( $\pm 0.003$ )	+0.258 ( $\pm 0.002$ )	65 ( $\pm 1$ )	65 ( $\pm 1$ )
Burchart	+0.32	+0.32	+0.32	+0.35	47.8	47.8
BKS	+0.38	+0.38	+0.38	+0.44	63.8	63.8
Universal	+0.11	+0.11	+0.11	+0.16	167.9	167.9
CVFF	+0.19	+0.19	+0.19	+0.21	107.6	107.6

Experimentally  $\alpha$ -cristobalite has two negative ( $\nu_{xz}$  ( $= \nu_{yz}$ ) and  $\nu_{zx}$  ( $= \nu_{zy}$ )) and one positive ( $\nu_{xy}$  ( $= \nu_{yx}$ )) on-axis Poisson's ratios. Furthermore, the calculated average polycrystalline isotropic aggregate Poisson's ratio ( $\nu_{\text{Voigt}}$ ), calculated using the Voigt method,<sup>[32]</sup> is also negative. The CVFF force field reproduces these trends and gives reasonable agreement with the absolute values. None of the other force fields reproduces the negative on-axis Poisson's ratios although both the BKS and, in particular, the Burchart force field predict low positive values of  $\nu_{xz}$  and  $\nu_{zx}$ . The BKS force field also predicts a negative  $\nu_{\text{Voigt}}$ . The BKS and Burchart force fields also give the closest agreement with the on-axis Young's moduli. The Universal force field gives the poorest agreement with the experimental on-axis Poisson's ratios and Young's moduli.

Figure 1 shows the off-axis variation in  $\nu_{yz}$  for  $\alpha$ -cristobalite due to rotation about the  $x$ -axis. Experimentally a negative value is maintained throughout full rotation about the  $x$ -axis, which is again only reproduced by the CVFF force field. However, all four force fields give the correct shape for the off-axis variation and the Burchart and BKS force field are negative for almost all rotation angles. The Universal force field again gives the poorest correlation with experiment, being positive for nearly all rotation angles.

The predicted value of the Poisson's ratios of SOD are  $\nu_{ij}$  ( $i, j = x, y, z$ ) = +0.32 (Burchart force field), +0.38 (BKS force field), +0.11 (Universal force field), and +0.19 (CVFF force field) compared with the experimental value of +0.30.<sup>[32]</sup> Hence in the case of SOD the Burchart force field gives the best agreement with the experimental Poisson's ratio, closely followed by the BKS and CVFF force fields. The Universal force field again fares the worst of the four force fields stud-

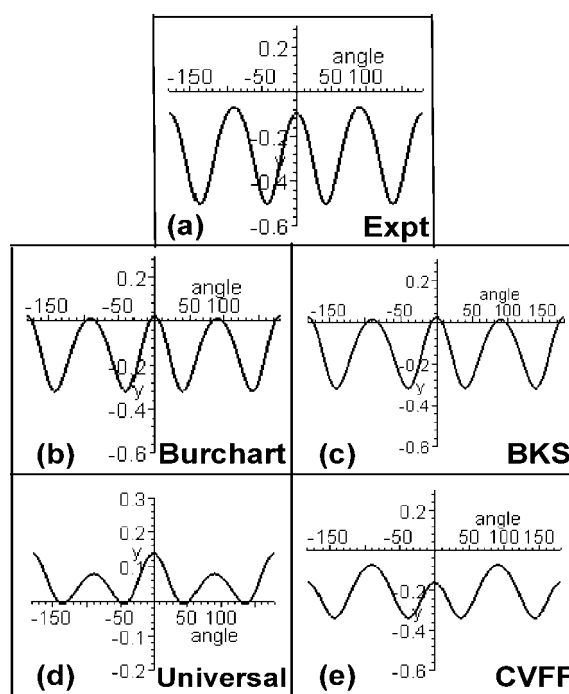


Fig. 1. Off-axis  $\alpha$ -cristobalite  $\nu_{yz}$  variations for rotation about the  $x$ -axis: a) experimental, b) Burchart force field, c) BKS force field, d) Universal force field, e) CVFF force field.

ied. Similar observations are found in the comparison of the predicted and experimental Young's moduli for SOD.

Independently of the force field or method used, negative Poisson's ratios (or very low positive) have been predicted for several idealized zeolite framework geometries—see Table 2. In general the all-silica equivalent structures exhibited larger negative values than the actual aluminosilicate and aluminophosphate structures. Some common structural features were observed in the zeolite structures exhibiting negative and low positive Poisson's ratios.

Negative Poisson's ratios were predicted in the (001) plane of THO (thomsonite—Al<sub>20</sub>Si<sub>20</sub>O<sub>80</sub>) (see Table 2). The THO framework is shown in Figure 2a. THO has a framework geometry in the (001) plane that may be described in terms of squares connected at their vertices, as illustrated in Figure 2b. In the idealized case where the squares are assumed to be rigid and connected through simple hinges at their vertices, the structure is geometrically constrained to have a constant in-plane Poisson's ratio of -1, as illustrated in Figure 2c.<sup>[34]</sup> If the constraint that the squares remain rigid is gently relaxed, then the Poisson's ratio becomes less negative and becomes dependent on the orientation in the plane, as observed for THO (see Fig. 3a). The "rigid square" in THO is achieved through the presence of cage-like structures containing eight-membered rings. Flexible Si—O—Al linkages act as hinges.

Other zeolites with a similar framework geometry are also predicted to exhibit auxetic behavior. The strong relationship between the Poisson's ratio and the nanostructure may be illustrated through examining the off-axis Poisson's ratios in NAT (natrolite—Al<sub>16</sub>Si<sub>24</sub>O<sub>80</sub>) and THO. The main structural

Table 2. Poisson's ratios for selected idealized zeolite structures (THO =  $\text{Al}_{20}\text{Si}_{20}\text{O}_{80}$ ; NAT =  $\text{Al}_{16}\text{Si}_{24}\text{O}_{80}$ ; APD =  $\text{Al}_{16}\text{P}_{16}\text{O}_{64}$ ; JBW =  $\text{Al}_{12}\text{Si}_{12}\text{O}_{48}$ ; AET =  $\text{Al}_{36}\text{P}_{36}\text{O}_{144}$ ; MFI =  $\text{Si}_{96}\text{O}_{192}$ ). Calculated errors are  $\pm 5\%$ .

		Burchart		BKS		CVFF		Universal	
		All-silica	Original	All-silica	Original	All-silica	Original	All-silica	Original
THO (001) plane	$\nu_{xy}$	-0.64	-0.55	-0.55	-0.33	-0.56	-0.46	-0.35	-0.33
	$\nu_{yx}$	-0.65	-0.55	-0.59	-0.53	-0.57	-0.46	-0.40	-0.40
NAT (001) plane	$\nu_{xy}$	-0.22	0.00	+0.10	+0.08	-0.16	+0.04	+0.09	+0.11
	$\nu_{yx}$	-0.22	0.00	+0.20	+0.22	-0.16	+0.04	+0.09	+0.10
APD (010) plane	$\nu_{xz}$	+0.03	+0.65	+0.55	+0.59	-0.06	+0.40	+0.81	+0.61
	$\nu_{zx}$	+0.03	+0.63	+0.91	+0.81	-0.07	+0.41	+0.81	+0.57
JBW (010) plane	$\nu_{xz}$	-0.16	-0.08	+0.13	+0.11	-0.02	+0.06	+0.07	+0.07
	$\nu_{zx}$	-0.38	-0.18	+0.19	+0.15	-0.18	+0.09	+0.17	+0.17
AET (100) plane	$\nu_{yz}$	-0.01	-0.09	-0.28	-0.32	-0.11	+0.02	-0.02	+0.03
	$\nu_{zy}$	-0.01	-0.11	-0.37	-0.42	-0.13	+0.03	-0.03	+0.03
MFI (010) plane	$\nu_{xz}$	+0.08		-0.14		-0.02		-0.08	
	$\nu_{zx}$	+0.08		-0.35		-0.02		-0.06	
MFI (100) plane	$\nu_{yz}$	+0.46		+0.35		+0.30		+0.54	
	$\nu_{zy}$	+0.34		+0.38		+0.27		+0.38	

difference between these zeolites on looking down the [001] direction is their alignment in the (001) plane. This structure similarity is perfectly illustrated through having virtually identical off-axis Poisson's ratio polar plots, except that they are out of phase with an angle that relates to their difference in alignment, as illustrated in Figures 3a and b.

Auxetic behavior is also predicted in the (010) plane of APD ( $\text{Al}_{16}\text{P}_{16}\text{O}_{64}$ , see Fig. 3c). The projected framework geometry in the (010) plane can once again be described in terms of the hinged rotating squares model. The "rigid squares" in APD are the result of eight-membered rings aligned parallel to the (010) plane and stacked down the [010] direction to form a column-like structure. Adjacent rings are interconnected through an oxygen atom, which acts as the hinge. Once again good correlation between the in-plane Poisson's ratios and the framework geometry is observed. Maxi-

mum auxeticity is achieved on loading in the [110] and  $[\bar{1}\bar{1}0]$  directions, which correspond to the framework being aligned as illustrated schematically in Figure 2c. Zeolites with similar nanostructures are also predicted to exhibit auxetic behavior.

In analogy to the "rotating squares" mechanism, a structure containing rigid equilateral triangles connected through simple hinges at their vertices is geometrically constrained to have a constant in-plane Poisson's ratio of  $-1$ , as illustrated in Figure 4. This type of geometry is also found in some zeolite frameworks for which force-field-based simulations predict a negative Poisson's ratio in the plane containing the triangles. For example, the Burchart force field predicts Poisson's ratios of  $\nu_{xz} = -0.082$  and  $\nu_{zx} = -0.181$  for JBW ( $\text{Al}_{12}\text{Si}_{12}\text{O}_{48}$ ), which has a framework geometry in the (010) plane (Fig. 4b) similar to that of the "rotating triangles" tessellation (Fig. 4a).

Negative Poisson's ratios were also predicted in some aluminophosphates where the auxetic behavior arises from re-orientation of the  $\text{PO}_4$  and  $\text{AlO}_4$  tetrahedra. For example, the four force fields have suggested negative or low positive Poisson's ratios for the (100) plane of AET ( $\text{Al}_{36}\text{P}_{36}\text{O}_{144}$ ), as listed in Table 2. The framework geometry in the (100) plane of AET is characterized by a zigzag pattern.

We have already noted that the Voigt method for calculating the Poisson's ratio of an isotropic polycrystalline aggregate from the experimental single-crystal elastic constants yields a negative Poisson's ratio for  $\alpha$ -cristobalite. It has also been shown elsewhere that the alternative Reuss method yields a negative polycrystalline isotropic Poisson's ratio.<sup>[9]</sup> In

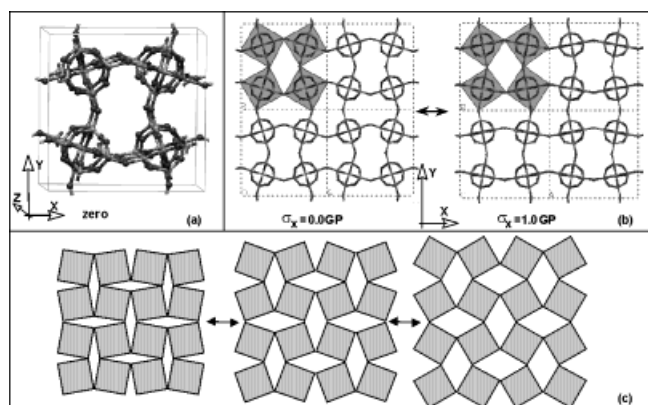


Fig. 2. Auxetic rotating squares: a) 3D THO framework, b) minimum energy configurations of the (001) plane in THO at different uniaxial loads in the x-direction, and c) the idealized rotating "hinging squares" mechanism.

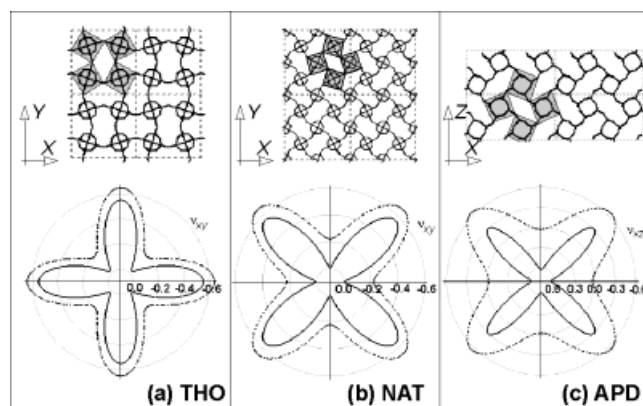


Fig. 3. Off-axis Poisson's ratios: the nanostructure of a) THO, b) NAT, and c) APD in planes where auxetic behavior is predicted together with the off-axis Poisson's ratio plots on axis rotation about a perpendicular axis (calculated using the Burchart force field). The auxetic behavior in all these three zeolites may be explained through the "rotating squares" microstructure. Note the excellent agreement between the framework alignment and the plots. Solid and dashed curves correspond to the original and all-silica equivalent structures, respectively.

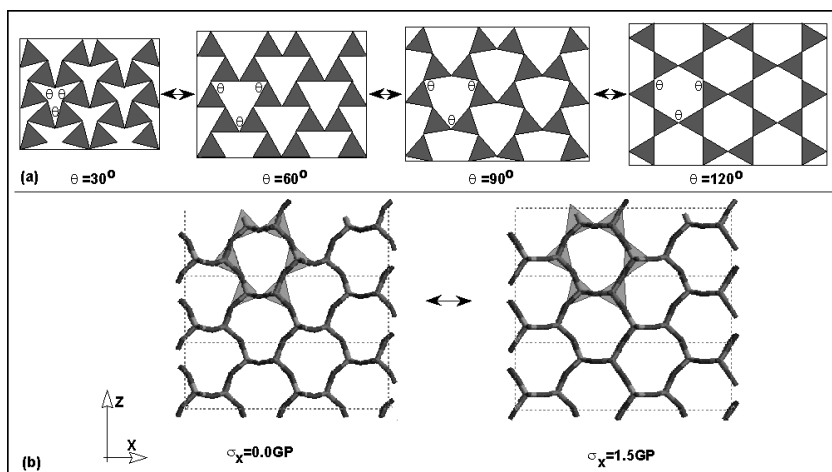


Fig. 4. Auxetic rotating triangles. a) The idealized model for achieving auxetic behavior from hinged rotating rigid equilateral triangles, and b) the (010) plane in JBW under different loads in the  $x$ -direction (horizontal). The different configurations in a) may be obtained by loading in a uniaxial direction.

both methods values are calculated for the isotropic bulk and shear moduli ( $K$  and  $G$ , respectively) and the Poisson's ratio is then calculated from the expression relating  $\nu$  to  $K$  and  $G$  for isotropic materials:  $\nu = (3K - 2G)/(6K + 2G)$ . We have performed similar analyses of the elastic constants predicted in our simulations on idealized zeolite structures. In order to calculate the upper and lower bounds of  $\nu$  in each case we note that the Voigt method calculates the least upper bounds of  $K$  and  $G$  whilst the Reuss method calculates the highest lower bounds of  $K$  and  $G$ .<sup>[33]</sup> Hence to calculate the upper bound on  $\nu$  we used the Voigt  $K$  and Reuss  $G$ , and for the lower bound on  $\nu$  we used the Reuss  $K$  and Voigt  $G$ . Negative isotropic polycrystalline aggregate Poisson's ratios were calculated in several cases. For example, calculations employing the Burchart force field yielded the following ranges:  $-0.36 \leq \nu_{\text{all-silica}}^{\text{APD}} \leq -0.09$ ;  $-0.01 \leq \nu_{\text{original}}^{\text{APD}} \leq +0.17$ ;  $-0.19 \leq \nu_{\text{all-silica}}^{\text{NAT}} \leq +0.18$ ;  $-0.06 \leq \nu_{\text{original}}^{\text{NAT}} \leq +0.23$ ;  $-0.14 \leq \nu_{\text{all-silica}}^{\text{THO}} \leq +0.20$ ;  $-0.03 \leq \nu_{\text{original}}^{\text{THO}} \leq +0.23$ .

It is interesting to note that the calculated isotropic polycrystalline aggregate Poisson's ratio for the all-silica equivalent APD structure,  $\nu_{\text{all-silica}}^{\text{APD}}$ , is calculated to be negative (see above) even though low positive on-axis Poisson's ratios are calculated for the single crystal case (Table 2). Figure 3c shows that this is due to the presence of negative off-axis Poisson's ratios for almost all rotation angles (about the  $y$ -axis), leading to an overall negative Poisson's ratio when all orientations are considered in the averaging process for a polycrystalline aggregate. The presence of a negative isotropic polycrystalline aggregate Poisson's ratio indicates that benefits and enhancements due to the auxetic property may be more easily achievable for the aggregate than for the single crystal case where crystal orientation needs to be accounted for in order to ensure the auxetic property is utilized effectively.

We have used a number of force fields that are well established for the prediction of zeolite properties, and have employed partial charges and/or the charge equilibration pro-

cedure to ensure charge neutrality in the absence of cations within the framework cage structures. We have also modeled all-silica equivalents of the zeolite structures in a further attempt to circumvent the charge neutralization issues for idealized (empty) zeolite framework geometries. These molecular modeling predictions strongly suggest that auxetic behavior occurs in a significant number of idealized zeolite structures, with the effect being related to the geometry and deformation mechanisms of the framework nanostructures.

The all-silica hypothetical analogues are also predicted to be auxetic, and are in general predicted to be more auxetic than the real structures. The all-silica analogues have the advantage that, due to possessing a neutral charge, no cations would be expected within the framework cavities. For the actual

structures where cations would be required to counteract the charged framework then it is necessary to consider what effect guest cation molecules would have on the elastic constants thus calculated. This has been investigated using interatomic potentials to model the elastic constants of the all-silica dodecasil-3C structure without guest molecules.<sup>[35]</sup> Comparison of these predicted values with experimental data for dodecasil-3C with guest molecules  $\text{N}_2$ , Ar, and  $\text{N}(\text{CH}_3)_3$  in the framework cages imply that only a small effect on the elastic constants is expected due to the presence of guest molecules.<sup>[35]</sup>

The existence of auxetic zeolites indicates that the benefits in employing auxetic materials as sieve materials<sup>[12,19]</sup> may potentially also be realized at the molecular level. For example, it can be shown through simple geometric analysis that for a sieve corresponding to the idealized "rotating squares" geometry illustrated in Figure 2, the radius of spheres that are allowed to pass through the filter<sup>[36]</sup> increases with an increase in the tensile stress, as illustrated in Figure 5a.

To further demonstrate the potential of auxetic zeolites in separations technologies we have performed simulations for the sorption of benzene and neopentane sorbate molecules onto the MFI ( $\text{ZSM5-Si}_96\text{O}_{192}$ ) zeolite all-silica structure. MFI has high Si/Al ratios and so charge issues are not so important in this case. The all-silica structure ( $\text{Si/Al} = \infty$ ) modeled here is also referred to as the silicalite structural isotype of MFI. MFI is predicted by the BKS force field to have both positive and negative Poisson's ratios for loading in the  $z$ -direction ( $\nu_{zx} = -0.35$  and  $\nu_{zy} = +0.38$ —see Table 2). The loading of neopentane molecules relative to benzene molecules as a function of tensile stress along the  $z$ -direction is also shown in Figure 5. At low stresses benzene molecules dominate the loading of MFI. This is consistent with experimental observation that the larger neopentane molecules (kinetic diameter 6.2 Å) are excluded from this structure whereas the smaller (5.85 Å) benzenes are not.<sup>[37]</sup> However, the neopentane loading is predicted to become comparable

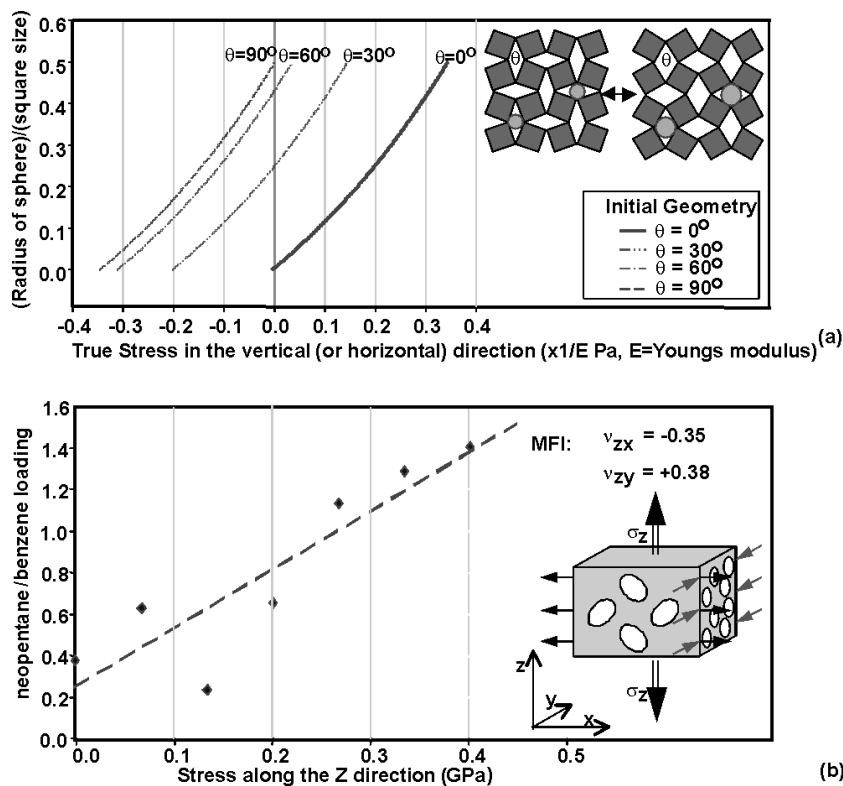


Fig. 5. Auxetic sieves: a) the relationship between uniaxial stress in an auxetic sieve with the “rotating squares” geometry and the radius of spherical particles that may pass through it, and b) the relationship between the sorbed neopentane/benzene ratio and stress in the z-direction for the auxetic zeolite MFI.

with that of benzene as the tensile stress in increased, to the extent that neopentane loading dominates benzene in the range  $0.25 < \sigma_z < 0.4$  GPa. We attribute this behavior to two effects: i) the opening up of the channels along  $y$  (due to the negative  $\nu_{zx}$ ) allowing the initially excluded neopentanes to be included; ii) the closing up of the channels along  $x$  (due to the positive  $\nu_{zy}$ ) tending to exclude the benzene molecules in these channels (see Fig. 5). The potential for using zeolites in tunable and selective sieving and switching devices is, therefore, clearly demonstrated.

To summarize, we have used force-field-based molecular simulations as a first approximation to predict negative Poisson's ratios in a number of idealized zeolite cage structures. The negative Poisson's ratios can in some cases be explained by simple geometry-deformation mechanism relationships. Notwithstanding charge neutralization, polarization, and guest molecule issues, the simulations on the idealized structures strongly suggest real zeolite single (and poly-) crystals may be auxetic. Previously demonstrated benefits from using auxetic materials as filters at the macroscopic and microscopic scales have also been demonstrated using force-field-based simulations on an idealized zeolite single crystal at the molecular level for the first time.

It will be necessary to verify these predictions through experimental measurement of the elastic constants of single-crystal zeolites. This is, of course, not trivial due to the typically small size of zeolite single crystals, although synthesis

routes for giant zeolite crystals (with dimensions in the millimeter range) have been reported.<sup>[20]</sup> The use of auxetic zeolites in molecular sieve applications is also a serious experimental challenge that may be more easily overcome with robust polycrystalline aggregates if the isotropic average Poisson's ratio is negative, or by using oriented zeolite single-crystal membranes on a substrate support where mechanical deformation of the aligned zeolite crystals is caused by expansion (thermal or mechanical) of the underlying substrate material.

The role of the framework geometry and deformation mechanisms in determining the nature of the Poisson's ratio leads us to speculate that auxetic behavior may also exist in other related structures, such as zeotypes (i.e., silico-alumino-phosphates and metal-silico-alumino-phosphates, etc.), and is worthy of further exploration.

### Experimental

**Molecular Modeling Simulations:** The starting structures, without cations present, were as provided within the Cerius<sup>2</sup> library of zeolite structures and are derived from experimental data. Energy expressions, including a term for coulomb interactions, were then set up and neutral unit cells attained as described in the following.

For the Burchart and BKS force fields the fixed charges supplied within the force fields were scaled until a neutral unit cell was attained. In the case of the CVFF force field the charges were calculated using the bond increment method using parameters supplied with the force field. For the Universal force field the charges were calculated using the charge equilibration procedure [30]. For purely siliceous frameworks it was, of course, not necessary to perform the aforementioned charge neutralization procedures. The non-bond interactions for all four force fields were summed using the Ewald summation procedure to minimize cut-off errors [38]. This procedure was used with automated cut-offs, and employs the geometric rule to compute the van der Waals energy term coefficients. Unloaded equilibrium minimum energy configurations were then derived by minimizing the force field derived potential energy as a function of the atomic coordinates to the earliest of the default Cerius<sup>2</sup> standard convergence criterion (atomic root mean square of 0.1 Kcal/mol) or 100 minimization steps with the unit-cell symmetry as observed experimentally. This was performed in order to guide the minimization towards the correct minimum, which proved to be essential in the case of the BKS force field where no formal “bonds” are included in the energy expression. The unit-cell symmetry was then reduced to  $P1$  and the structures were minimized again to the earlier of the default Cerius<sup>2</sup> high convergence criterion (atomic RMS of 0.001 Kcal/mol) or 5000 minimization steps. This step was repeated three times to enable re-calculation of the non-bond list. In general, convergence was achieved within the first 5000 steps. The stiffness matrix  $C$  was then computed from the second derivative of the energy expression [39] since the terms  $c_{ij}$  in the stiffness matrix are related to the potential energy function  $V$  through  $c_{ij} = \partial^2 V / \partial \epsilon_i \partial \epsilon_j$ .

Sorption simulations were performed at a sorption temperature of 300 K. The Yashonath sorption force field [40] was employed, which is designed for sorption of rigid small molecules onto zeolite structures. Simulations were performed using the “fixed pressure” method, which is a grand canonical Monte Carlo method in which the sorbate molecule positions and orientations are varied and sorbates are allowed to be created and destroyed. Benzene and neopentane sorbates were used simultaneously, firstly on the minimized undeformed structure and then on several minimized structures subject to loading in the z-direction in increments of 0.067 GPa up to 0.402 GPa.

Received: February 3, 2000  
Final version: August 15, 2000

- [1] R. Lakes, *Science* **1987**, 235, 1038.  
 [2] K. E. Evans, *Chem. Ind.* **1990**, 654.  
 [3] B. D. Caddock, K. E. Evans, *J. Phys. D: Appl. Phys.* **1989**, 22, 1877.  
 [4] K. E. Evans, A. Alderson, F. R. Christian, *J. Chem. Soc., Faraday Trans.* **1995**, 91, 2671.  
 [5] K. E. Evans, M. M. Nkansah, I. J. Hutchinson, S. C. Rogers, *Nature* **1991**, 353, 124.  
 [6] R. H. Baughman, D. S. Galvao, *Nature* **1993**, 365, 735.  
 [7] C. B. He, P. W. Liu, A. C. Griffin, *Macromolecules* **1998**, 31, 3145.  
 [8] R. H. Baughman, J. M. Shacklette, A. A. Zakhidov, S. Stafstrom, *Nature* **1998**, 392, 362.  
 [9] A. Yeganeh-Haeri, D. J. Weidner, J. B. Parise, *Science* **1992**, 257, 650.  
 [10] N. R. Keskar, J. R. Chelikowsky, *Nature* **1992**, 358, 222.  
 [11] K. L. Alderson, A. P. Pickles, P. J. Neale, K. E. Evans, *Acta Metall. Mater.* **1994**, 42, 2261.  
 [12] A. Alderson, K. E. Evans, J. Rasburn, *World Patent WO 99/22 838*, **1999**.  
 [13] A. Alderson, *Chem. Ind.* **1999**, 384.  
 [14] B. Smit, T. L. M. Maisen, *Nature* **1995**, 374, 42.  
 [15] S. I. Zones, M. E. Davis, *Curr. Opin. Solid State Mater. Sci.* **1996**, 1, 107.  
 [16] A. E. H. Love, *A Treatise on the Mathematical Theory of Elasticity*, 4th ed., Cambridge University Press, Cambridge **1944**.  
 [17] H. J. McSkimin, P. Andreatch, Jr., R. N. Thurston, *J. Appl. Phys.* **1965**, 36, 1624.  
 [18] W. A. Smith, in *Proc. IEEE Ultrasonics Symp.*, IEEE Publications, Piscataway, NJ **1991**, p. 661.  
 [19] A. Alderson, J. Rasburn, S. Ameer-Beg, P. G. Mullarkey, W. Perrie, K. E. Evans, *Ind. Eng. Chem. Res.* **2000**, 39, 654.  
 [20] A. Kuperman, S. Nadimi, S. Oliver, G. A. Ozin, J. M. Garcés, M. M. Olken, *Nature* **1993**, 365, 239.  
 [21] M. J. Sanders, M. Leslie, C. R. A. Catlow, *J. Chem. Soc. Chem. Commun.* **1984**, 1273.  
 [22] R. A. Jackson, S. C. Parker, P. Tschaufeser, in *Modelling of Structure and Reactivity of Zeolites* (Ed: C. R. A. Catlow), Academic, London **1992**.  
 [23] J. D. Gale, A. K. Cheetham, *Zeolites* **1992**, 12, 674.  
 [24] J. D. Gale, N. J. Henson, *J. Chem. Soc., Faraday Trans.* **1994**, 90, 3175.  
 [25] Cerius<sup>2</sup> V3.0, MSI Inc., San Diego, CA **2000**.  
 [26] R. F. S. Hearmon, *An Introduction to Applied Anisotropic Elasticity*, Oxford University Press, Oxford **1961**.  
 [27] E. Vos Burchart, *Ph.D. Thesis*, Delft University of Technology, The Netherlands **1992**, Table I, Ch. XII.  
 [28] B. W. H. Van Beest, G. J. Kramer, R. A. Van Santen, *Phys. Rev. Lett.* **1990**, 64, 1955.  
 [29] A. K. Rappe, C. J. Casewit, K. S. Colwell, W. A. Goddard, W. M. Skiff, *J. Am. Chem. Soc.* **1992**, 114, 10046.  
 [30] A. K. Rappe, W. A. Goddard, *J. Phys. Chem.* **1991**, 95, 3358.  
 [31] *Force-Field Based Simulations Cerius<sup>2</sup> User Guide*, MSI Inc., San Diego, CA **1996**.  
 [32] Z. Li, M. V. Nevitt, S. Ghose, *Appl. Phys. Lett.* **1989**, 55, 1730.  
 [33] G. Simmons, H. Wang, *Single Crystal Elastic Constants and Calculated Aggregate Properties: A Handbook*, 2nd ed., MIT Press, Cambridge, MA **1971**.  
 [34] J. N. Grima, K. E. Evans, *J. Mater. Sci. Lett.* **2000**, 19, 1563.  
 [35] K. de Boer, A. P. J. Jansen, R. A. Van Santen, S. C. Parker, *Phys. Rev. B* **1996**, 53, 14073.  
 [36] J. N. Grima in *New Auxetic Materials*, Ph.D. Thesis, University of Exeter, UK **2000**, Ch. 4.  
 [37] E. M. Flanigen, J. M. Bennett, J. W. Grose, J. P. Cohen, R. L. Patton, R. M. Kirchner, J. V. Smith, *Nature* **1978**, 271, 512.  
 [38] N. Karasawa, W. A. Goddard, *J. Phys. Chem.* **1989**, 93, 7320.  
 [39] *Cerius<sup>2</sup> Property Prediction*, MSI Inc., San Diego, CA **1997**.  
 [40] S. Yashonath, J. M. Thomas, A. K. Nowak, A. K. Cheetham, *Nature* **1988**, 331, 601.

## Imaging the Absolute Polar Molecular Orientation with Monolayer Sensitivity\*\*

By Mathias Flörsheimer,\* Maik-Thomas Bootsmann, and Harald Fuchs

Polar order occurs naturally at interfaces due to the asymmetric interaction of the molecules with the adjacent bulk phases. The unique geometrical arrangement and orientation of the molecules directly at an interface<sup>[1–4]</sup> is of key importance in understanding many phenomena, such as crystal growth, heterogeneous catalysis, electrochemical reactions, and corrosion. In contrast to the order at interfaces, most bulk materials exhibit centrosymmetric point groups, in which the dipole–dipole interaction energy between the molecules is minimized.<sup>[5]</sup> Polar bulk materials are key elements in many technological applications, for example, for optical frequency conversion<sup>[6–8]</sup> or high-speed electro-optic modulation<sup>[9]</sup> of light. A strategy for the development of novel, highly efficient polar materials is to start from a polar monolayer at an interface and to grow its specific order into the third dimension by applying techniques such as organic molecular beam deposition<sup>[10]</sup> (OMBE) or Langmuir–Blodgett<sup>[11]</sup> (LB) film transfer. In order to control the quality of the growing films, techniques for the measurement of the polar order and its spatial distribution are needed. Simple linear optical techniques do not allow axial and polar order to be distinguished. However, if the sample is illuminated with high-intensity laser light, a second-harmonic (SH) signal can be generated that exhibits phase information about the absolute molecular orientation. Here, we demonstrate the feasibility of imaging this information with monolayer sensitivity.

The phase-sensitive SH microscope described here is an improvement of an SH imaging technique we used recently to characterize interfaces.<sup>[12–14]</sup> In this latter microscope, the spatial distribution of the SH intensity generated at an interface is imaged. The pictures can be quantitatively interpreted in terms of the lateral distribution of symmetry and order. But this technique does not take advantage of the full information in the SH signal because the phase is obscured in the intensity measurement. This means that the molecular orientation can be determined only with an uncertainty of 180° (axial orientation). Below, we first describe the principle of SH intensity imaging, then we introduce our phase-sensitive SH microscope for the determination of the absolute molecular orientation.

Figure 1a shows schematically the principle of our intensity contrast SH microscope in the simplest version.<sup>[13]</sup> The specimen may be, for example, a liquid/air interface. The topmost

\*] Dr. M. Flörsheimer, M.-T. Bootsmann, Prof. H. Fuchs  
 Physikalisches Institut, Universität Münster  
 Wilhelm-Klemm-Strasse 10, D-48149 Münster (Germany)  
 E-mail: florshl@nvwz.uni-muenster.de

\*\*] Financial support from the Volkswagen Foundation and the Federal Ministry for School, Advanced Education, Science and Research of Northrhine-Westphalia is gratefully acknowledged.